

## Article

# Efficient Synthesis of Imine-Carboxylic Acid Functionalized Compounds: Single Crystal, Hirshfeld Surface and Quantum Chemical Exploration

Muhammad Nawaz Tahir <sup>1</sup>, Akbar Ali <sup>2,\*</sup> , Muhammad Khalid <sup>3,4,\*</sup> , Muhammad Ashfaq <sup>1</sup> , Mubashir Naveed <sup>1</sup>, Shahzad Murtaza <sup>3,4</sup> , Iqra Shafiq <sup>3,4</sup> , Muhammad Adnan Asghar <sup>5</sup> , Raha Orfali <sup>6,\*</sup> and Shagufta Perveen <sup>7</sup> 

<sup>1</sup> Department of Physics, University of Sargodha, Sargodha 40100, Pakistan

<sup>2</sup> Department of Chemistry, Government College University Faisalabad, Faisalabad 38000, Pakistan

<sup>3</sup> Institute of Chemistry, Khwaja Fareed University of Engineering & Information Technology, Rahim Yar Khan 64200, Pakistan

<sup>4</sup> Centre for Theoretical and Computational Research, Khwaja Fareed University of Engineering & Information Technology, Rahim Yar Khan 64200, Pakistan

<sup>5</sup> Department of Chemistry, Division of Science and Technology, University of Education, Lahore 54770, Pakistan

<sup>6</sup> Department of Pharmacognosy, College of Pharmacy, King Saud University, P.O. Box 2457, Riyadh 11451, Saudi Arabia

<sup>7</sup> Department of Chemistry, School of Computer, Mathematical and Natural Sciences, Morgan State University, Baltimore, MD 21251, USA

\* Correspondence: akbarali@gcuf.edu.pk (A.A.); khalid@iq.usp.br (M.K.); rorfali@ksu.edu.sa (R.O.)

**Abstract:** Two aminobenzoic acid based crystalline imines (**HMBA** and **DHBA**) were synthesized through a condensation reaction of 4-aminobenzoic acid and substituted benzaldehydes. Single-crystal X-ray diffraction was employed for the determination of structures of prepared Schiff bases. The stability of super molecular structures of both molecules was achieved by intramolecular H-bonding accompanied by strong, as well as comparatively weak, intermolecular attractive forces. The comparative analysis of the non-covalent forces in **HMBA** and **DHBA** was performed by Hirshfeld surface analysis and an interaction energy study between the molecular pairs. Along with the synthesis, quantum chemical calculations were also accomplished at M06/6-311G (d, p) functional of density functional theory (DFT). The frontier molecular orbitals (FMOs), molecular electrostatic potential (MEP), natural bond orbitals (NBOs), global reactivity parameters (GRPs) and natural population (NPA) analyses were also carried out. The findings of FMOs found that  $E_{\text{gap}}$  for **HMBA** was examined to be smaller (3.477 eV) than that of **DHBA** (3.7933 eV), which indicated a greater charge transference rate in **HMBA**. Further, the NBO analysis showed the efficient intramolecular charge transfer (ICT), as studied by Hirshfeld surface analysis.

**Keywords:** single-crystal XRD; condensation reaction; Hirshfeld surface analysis; density functional theory; NBO analysis



**Citation:** Tahir, M.N.; Ali, A.; Khalid, M.; Ashfaq, M.; Naveed, M.; Murtaza, S.; Shafiq, I.; Asghar, M.A.; Orfali, R.; Perveen, S. Efficient Synthesis of Imine-Carboxylic Acid Functionalized Compounds: Single Crystal, Hirshfeld Surface and Quantum Chemical Exploration. *Molecules* **2023**, *28*, 2967. <https://doi.org/10.3390/molecules28072967>

Academic Editor: Athanassios C. Tsipis

Received: 15 February 2023

Revised: 11 March 2023

Accepted: 20 March 2023

Published: 27 March 2023



**Copyright:** © 2023 by the authors. Licensee MDPI, Basel, Switzerland. This article is an open access article distributed under the terms and conditions of the Creative Commons Attribution (CC BY) license (<https://creativecommons.org/licenses/by/4.0/>).

## 1. Introduction

In the modern world, scientists are trying to explore every possible aspect of newly synthesized chemical building blocks in order to find their maximum utility in the betterment of humanity. In this scenario, crystalline organic compounds are also considered to be important chemical building blocks as their synthesis and computational examination are substantially recognized in modern times. Imines (also called Schiff bases) are a significant class of chromophores produced by the condensation reaction of primary amines and carbonyl chromophores (ketones or aldehydes), causing azomethine ( $-C=N-$ ) formation [1]. Imines are vital class of organic compounds with numerous applications in the field of

coordination chemistry as the azomethine ( $-C=N-$ ) group is considered as the prized ligand for the production of numerous metal complexes of valuable interest [2,3]. Besides coordination chemistry, Schiff bases are strong candidates in analytical chemistry because of their significant applications in this field [4]. Moreover, the exploration of Imines in the field of medicinal chemistry has also been well recognized because of their potential as anticancer [5], anti-tubercular [6], analgesic and anti-inflammatory [7], antimicrobial [8,9], antioxidant [10,11], anthelmintic [12] and anticonvulsant medicines [13–17], etc. Imines derived from primary amines are basic in nature, while in acidic solution they readily convert in to iminium ions [18,19]. Iminium catalysis for the asymmetric organic transformation is another area where they are well recognized [20]. Iminium ion/imines/Schiff bases are the key intermediates in multi-component reactions (Ugi four-component procedure) as well as having remarkable roles in fabrication of alkaloids and various nitrogen-containing heterocyclic compounds [21–23]. One of the very important features of this functionality is its existence as a zwitterion or inner salt that contributes significantly towards the modification of physical properties, such as solubility enhancement and boasting permeability of the compounds; these are extremely appreciated features in the field of designing drugs [24]. On the other hand, carboxylic acids are a significant class of organic systems with multiple applications in the fields of agriculture, medicine, food, pharmaceuticals and other industries [25]. These organic acids and their derivatives are used in the production of biopolymers, polymers, coatings, pharmaceutical drugs, adhesives, solvents, antimicrobials, food additives, flavorings, etc. [26]. This is also a crucial class of organic chromophores with a number of advantages in the coordination chemistry arena, as the carboxylate functional moiety has been well analyzed as a valuable ligand for the production of numerous metal complexes of valuable interest [26–29]. The overlapping of discrete research grounds for the exploration, reasoning and investigation of the major electronic characteristics of the yielded organic systems is a recently acknowledged research area. In this context, density functional theory computations are greatly recognized as a significant method for the assessment of basic electronic characteristics of the recently manufactured chromophores, and, likewise, non-covalent interactions and nonlinear optical properties [30–32]. Functionalized azomethine have also been investigated by the DFT analysis for the detailed investigation of their key electronic properties [33].

Dual functionalized compounds such as 4-amino benzoic acid are excellent candidates for modification to valuable chemical architectures that, in turn, could be utilized for developing stabilized silver nanoparticles with potential analytical probes for the selective colorimetric sensing of  $Ni^{2+}$  ions and antimicrobial performance [34]. As our group is continuously working on the synthesis and DFT-based exploration of organic compounds belonging to different classes, here, we are showcasing our research relating to the synthesis, single-crystal investigation and DFT study of the carboxylic acid functionalized imine compounds: **DHBA** and **HMBA**. Furthermore, the free carboxylic acid functionality will further be applied for the production of valuable coordination compounds [35].

## 2. Result and Discussion

### 2.1. Description of SC-XRD Analysis of HMBA and DHBA

The crystal structure and the mode by which the molecules are packed in **HMBA** and **DHBA** are elaborated in a detailed way. The details related to the SC-XRD experiment are depicted in Tables S1–S3 (Supplementary Information) specify the bond lengths as well as the bond angles of **HMBA** and **DHBA** compared with the results of DFT.

The crystalline structure of **HMBA** has a 2- $\{(E)-[(4\text{-carboxyphenyl})\text{iminio}]\text{methyl}\}$ -6-methoxyphenolate (C1–C15/N1/O1–O4) and a methanol molecule (Figure 1a), whereas **DHBA** contains a (E)-4- $\{(2\text{-hydroxy-3,5-diodobenzylidene})\text{amino}\}$ benzoic acid (C1/C2A–C7A/C8–C14/N1/O1–O3/I1/I2) and a dimethyl sulfoxide (DMSO) molecule (Figure 1b). 2- $\{(E)-[(4\text{-carboxyphenyl})\text{iminio}]\text{methyl}\}$ -6-methoxyphenolate adopts the keto tautomeric form, whereas (E)-4- $\{(2\text{-hydroxy-3,5-diodobenzylidene})\text{amino}\}$ benzoic acid adopts the enol tautomeric form. In **HMBA**, the ring A (C1–C7/N1/O1/O2) and group B (C8–C15/O3/O4)

are roughly planar with a root mean square (r.m.s) deviation of 0.0800 and 0.0115 Å, with A/B dihedral angle of 8.7 (2)°. In **DHBA**, the phenyl ring (C2A-C7A) is refined as disordered over two positions by employing the equal anisotropic parameters of all the atoms involved in disorder, and the refined occupancy ratio is 0.538 (13):0.462 (13). In **DHBA**, the similar ring A (C1/C2A-C7A/N1/O1/O2) and group C (C8-C14/O3/I1/I2) are roughly planar with r.m.s deviations of 0.1116 and 0.0446 Å. The carboxylate group oxygen atom (O2) of group C showed maximum deviation from the plane with a deviation of 0.2322 (9) Å. The intramolecular N-H···O and O-H···N bonding are the primary characteristic of the molecular configuration of **HMBA** and **DHBA**, respectively. By the intramolecular H-bonding in **HMBA** and **DHBA**, the S (6) H-bonded loop is formed. There is some sort of similarity in the mode by which compounds are packed in both compounds. In both compounds, the main molecule is associated with the solvent molecule through O-H···O bonding. In **HMBA**, the 2-((E)-[(4-carboxyphenyl) iminio]methyl)-6-methoxyphenolate molecules are directly interconnected via C-H···O bonding; whereas, in **DHBA**, the (E)-4-((2-hydroxy-3,5-diiodobenzylidene)amino)benzoic acid molecules are not interlinked directly with each other via any sort of H-bonding, but these are linked through the DMSO molecule. In **HMBA**, the molecules are connected in the form trimer through O-H···O and C-H···O bonding to complete the R<sub>3</sub><sup>3</sup>(21) loop [36]. The trimers are further interlinked with each other through C-H···O bonding. The C (11) chains of molecules are formed via O-H···O and C-H···O bonding that run along the *b*-axis (Figure 2, Table 1). Similarly, in **DHBA**, the chains of molecules are formed via intermolecular O-H···O and C-H···O bonding (Figure S1 and Table 1). The weak  $\pi$ ··· $\pi$  stacking interactions among aromatic rings cause further strengthening of the crystalline packing of **HMBA** via inter-centroid separation of 4.600 (5) to 5.198 (5) Å; whereas, the C-I··· $\pi$  interaction with I··· $\pi$  distance of 3.783 Å (Figure 3) and  $\pi$ ··· $\pi$  stacking interaction via inter-centroid separation of 4.328 (6) to 5.849 (6) Å are responsible for the further strengthening of the crystal packing of **DHBA**. Moreover, a Cambridge structure database search was performed in order to find the closely related compounds. A general search of (E)-(4-(benzylideneamino) phenyl) methanol provides a lot of hints. Out of these hints, some very closely related compounds are found with the reference codes BZANPC10 [37], BZANPC11 [38], DIWMAY [39], FAXXIN [40], NEZXAT [41], PUSMUN [42]. A comparative study on geometrical parameters between DFT and XRD was also accomplished, and harmony between the values was examined (Tables S2 and S3 and Figure S5) which indicates the suitable selection of DFT functional for the current study.

## 2.2. Hirshfeld Surface Analysis

In the field of supramolecular chemistry, the need for the detailed survey of the non-covalent interactions is increasing day by day as it forms the basis of crystal packing. Herein, we are focused on exploring these interactions in the studied compounds via Hirshfeld surface analysis through Crystal Explorer v. 21.5 [43]. A Hirshfeld surface (HS), which is constructed on the basis on normalized distances ( $d_{\text{norm}}$ ), enables us to explore the hydrogen bonding interactions [31,44–47]. Red regions on the surface stand for the smaller interatomic contact, whereas blue parts stand for larger interatomic contacts. The region of white color of HS stands for the contacts in which the distance among the associated atoms is equal to the sum of the van der Waal radii of atoms. The red spots on HS for **HMBA** (Figure 3a) and **DHBA** (Figure 3b) indicate atoms that are involved in small interatomic contacts or in H-bonding interactions. Shape index is the property that is employed for plotting HS to explore  $\pi$ ··· $\pi$  interactions. The regions of red and blue having the shape of a triangle around the aromatic rings on HS (shape index) are the indicators of the  $\pi$ ··· $\pi$  stacking interactions in **HMBA** (Figure 3c) and **DHBA** (Figure 3d).

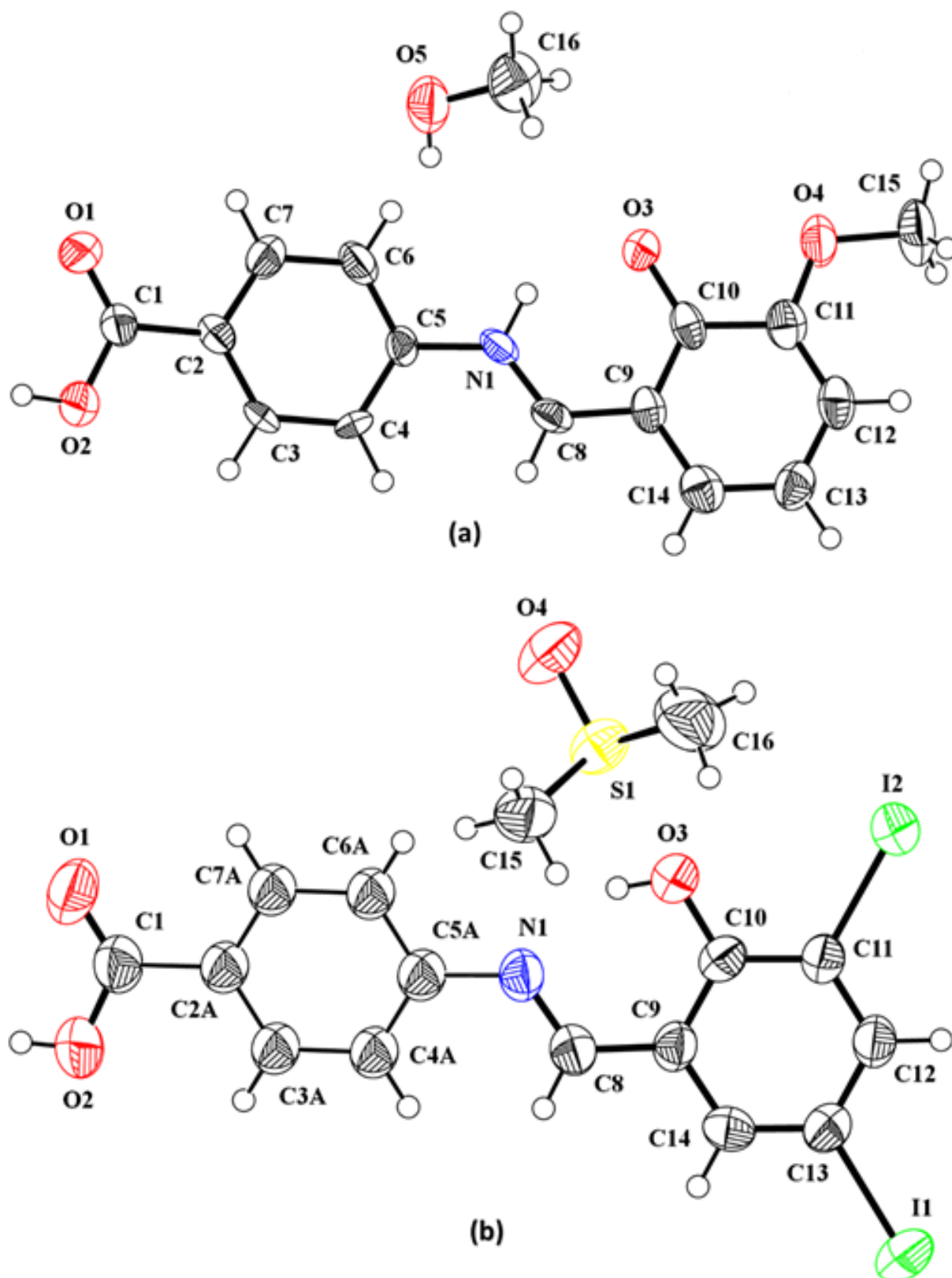


**Figure 1.** ORTEP diagram of (a) HMBA, (b) DHBA. Figures are portrayed at probability level of 50%. H-atoms are displayed by circles of arbitrary radii.

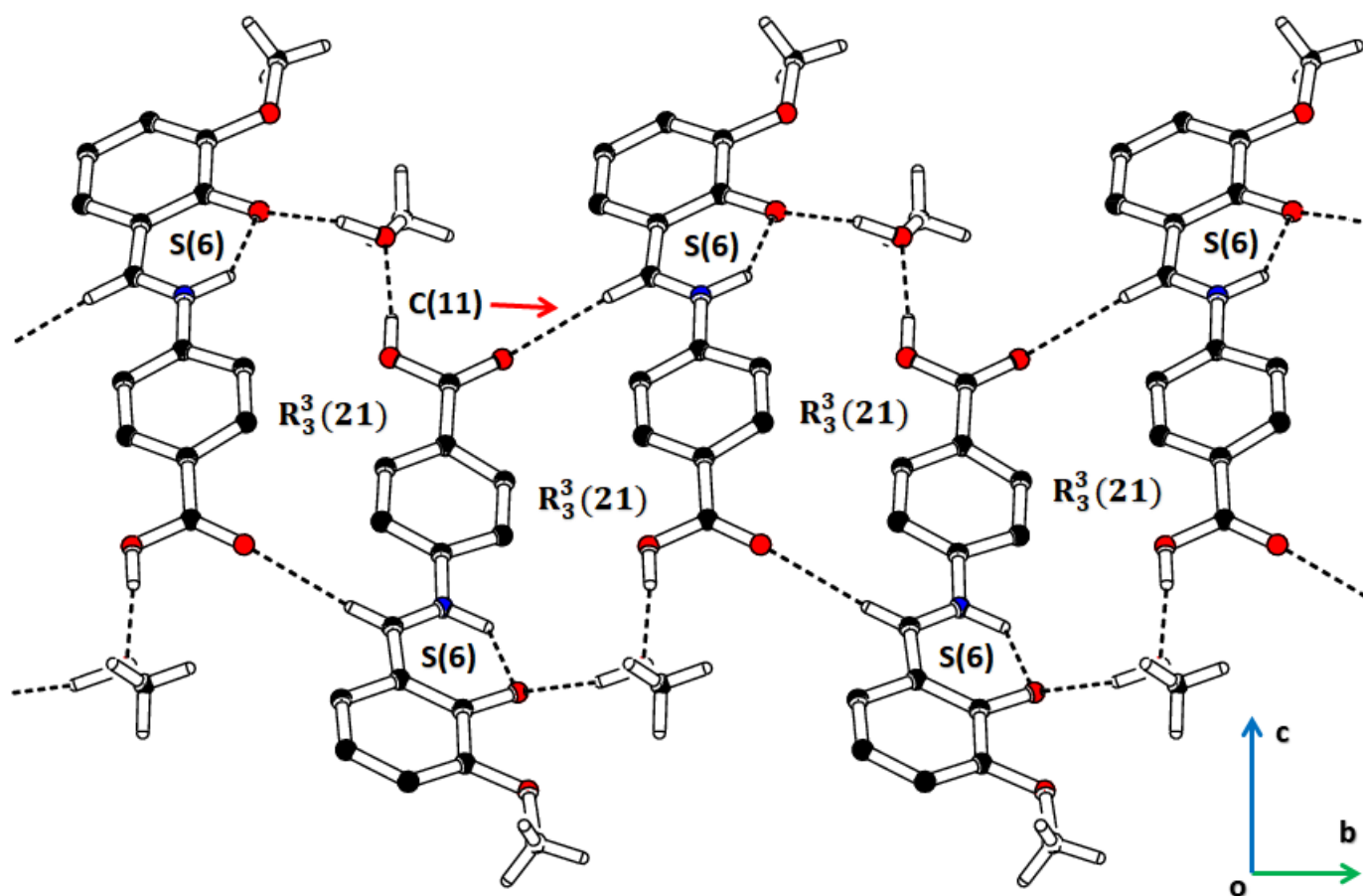


**Figure 2.** Packing diagram of HMBA showing intra and as well as intermolecular H-bonding. Selected H-atoms are represented for simplicity.

**Table 1.** Hydrogen-bond geometry ( $\text{\AA}$ ,  $^\circ$ ) for HMBA and DHBA with  $C-I\cdots\pi$  interaction for DHBA.

	$D-H\cdots A$	$D-H$	$H\cdots A$	$D\cdots A$	$\angle(D-H\cdots A)^\circ$
HMBA	$O2-H2\cdots O5^i$	0.89 (9)	1.76 (9)	2.628 (9)	164 (10)
	$N1-H1\cdots O3$	0.95 (8)	1.77 (8)	2.560 (8)	138 (7)
	$C8-H8\cdots O1^{ii}$	0.93	2.55	3.410 (11)	155
	$O5-H5A\cdots O3^{iii}$	0.82	1.98	2.765 (9)	159
	$O2-H2\cdots S1^i$	0.82	2.95	3.707 (4)	154
	$O2-H2\cdots O4^i$	0.82	1.81	2.601 (5)	162
DHBA	$O3-H3\cdots N1$	0.82	1.84	2.567 (5)	148
	$C8-H8\cdots O4^v$	0.93	2.55	3.445 (7)	162
	$C12-H12\cdots I2^{vi}$	0.93	3.19	4.090 (5)	163
	$C14-H14\cdots S1^v$	0.93	2.89	3.767 (6)	159
	$C15-H15A\cdots O3^{vii}$	0.96	2.57	3.290 (7)	132
	$C15-H15B\cdots O1^i$	0.96	2.36	3.247 (7)	154
	$C15-H15C\cdots O1^{iv}$	0.96	2.51	3.359 (7)	147
	$C-I\cdots\pi$	$C-I$	$I\cdots\pi$	$C\cdots\pi$	$\angle(C-I\cdots\pi)^\circ$
$C11-I2\cdots Cg1^{viii}$	2.083 (5)	3.783 (2)	4.338 (5)	90.62 (13)	

Symmetry codes: (i)  $-x, y - 1/2, -z + 1/2$ ; (ii)  $-x + 1, y - 1/2, -z + 1/2$ ; (iii)  $x - 1, y, z$ ; (iv)  $-x, y + 1/2, -z + 1/2$ ; (v)  $x, -y + 1/2, z + 1/2$ ; (vi)  $-x + 1, -y + 2, -z + 1$ ; (vii)  $x, y - 1, z$ ; (viii)  $x, y + 1, z$ . Cg1 is (C9–C14) ring for DHBA.

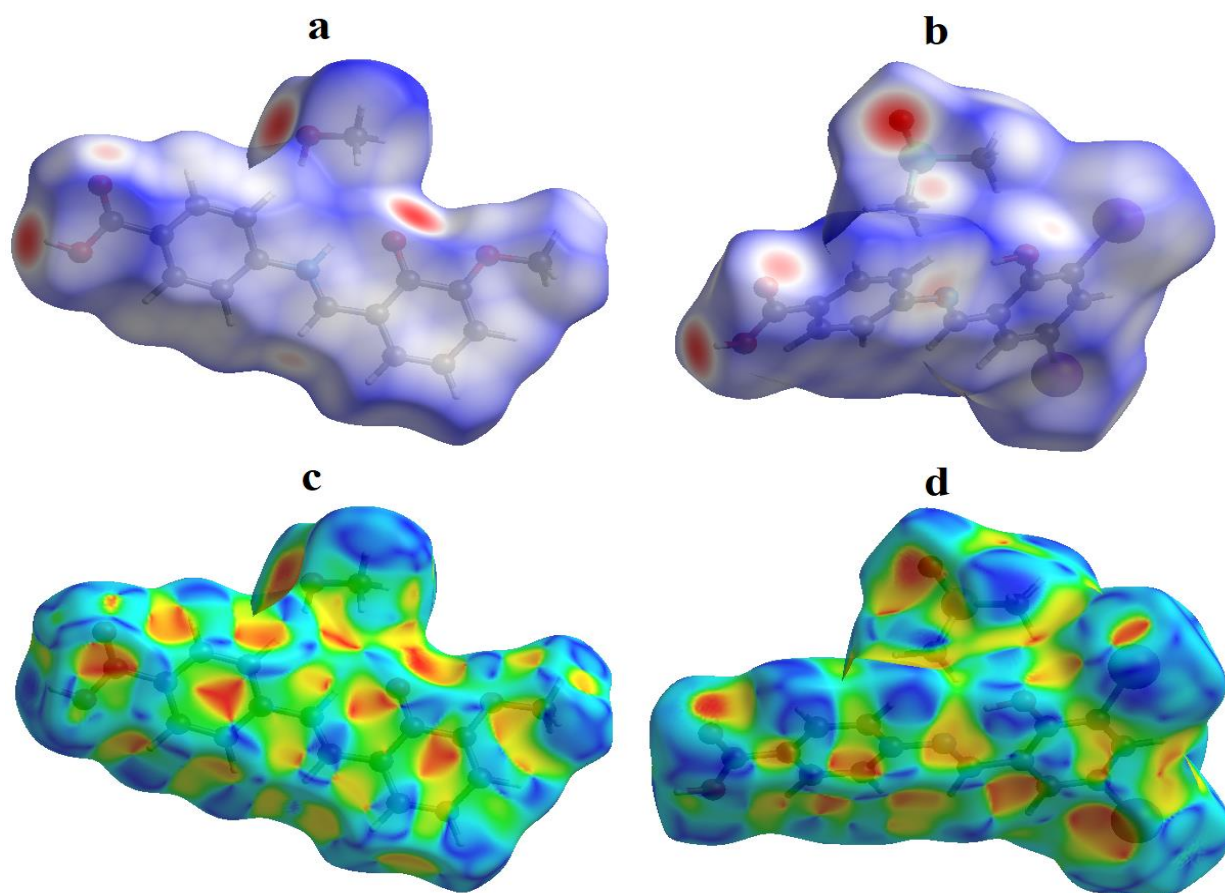


**Figure 3.** HS plotted over property dnorm for (a) **HMBA** in the range  $-0.7172$  to  $1.3189$  a.u., (b) **DHBA** in the range  $-0.7444$  to  $1.2641$  a.u. HS plotted over property shape index in the range  $-1$  to  $1$  a.u. for (c) **HMBA**, (d) **DHBA**.

The vital or precious interatomic contacts present in the crystal packing of single-crystals can be effectively explored by employing 2D finger print plots [48,49]. The plots for whole interactions are represented by Figure S4a for **HMBA** and Figure S4e for **DHBA**. The largest spikes on these plots stand for  $O \cdots H$  contact. A significant difference is found in the interatomic contacts of **HMBA** and **DHBA**. For **HMBA**, the contact of utmost importance is  $H \cdots H$  (42.2%, Figure S3a), whereas for **DHBA**, the contact of utmost importance is  $O \cdots H$  (24.3%, Figure S3f). The  $C \cdots H$  and  $O \cdots H$  contacts have substantial contributions in the crystal packing of both compounds which is the evidence of the  $C-H \cdots O$  bonding in them. The other interatomic contacts for **HMBA** and **DHBA** are shown by Figure S3a–d and Figure S3e–k, respectively. In order to make the study of short contacts more interesting, we computed the enrichment ratio for finding the tendency of the pair of the chemical species to form crystal packing associations for both compounds. The enrichment ratio is calculated by following the procedure created by the Christian Jelsch et al. [50]. The results of the enrichment ratio are exhibited in Table S4 for **HMBA** and Table S5 for **DHBA**. For **HMBA**, the contacts that are more favorable than other contacts are  $C \cdots C$ ,  $O \cdots H/H \cdots O$  with enrichment ratios of 2.52 and 1.43, respectively. For **DHBA**, the contacts that are more favorable than other contacts are  $I \cdots I$ ,  $S \cdots H/H \cdots S$ ,  $C \cdots C$  with enrichment ratios of 2.27, 1.92 and 1.48, respectively.  $C \cdots C$  contacts are favorable contacts in both compounds as both compounds contain aromatic rings.

In the exploration of the single crystals, the scientist tries to determine the strength of crystal packing. We also do the same by exploring the void analysis [51,52] of **HMBA** (Figure 4a) and **DHBA** (Figure 4b). All the atoms are supposed to be spherically symmetrical and the electron density of all the atoms is added up in order to find the voids. Overall,

148.02 Å<sup>3</sup> and 216.36 Å<sup>3</sup> are the calculated voids in **HMBA** and **DHBA**, respectively. The void in **HMBA** is 9.98% and in **DHBA** it is 11.4% which shows the absence of any sort of cavity in the crystalline packing of both compounds.

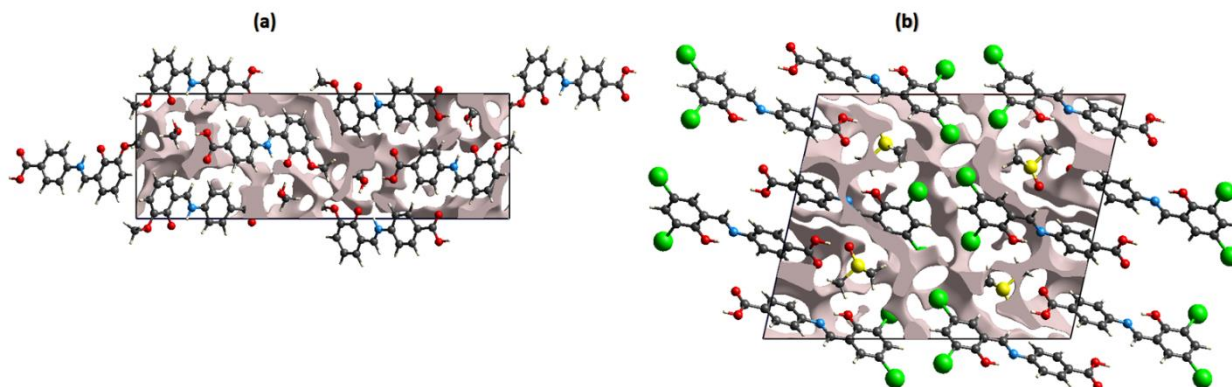


**Figure 4.** Graphical illustration of voids in (a) **HMBA** along a-axis, (b) **DHBA** along b-axis.

In order to further investigate the interactions in **HMBA** and **DHBA**, interaction energy between the main molecule and the solvent molecule is calculated on crystal explorer using the HF/3-21G electron density model. The intermolecular interaction energy is the sum of four kinds of energies named as electrostatic, dispersion, polarization and repulsion. The electrostatic energy can be attracted or repulsive. The strength of the interaction can be shown by the width of the cylinder connected with the center of the molecules. A larger width of the cylinder indicates a stronger interaction. In the case of **HMBA**, the roles of the electrostatic and dispersion energies in defining the total energy are almost the same. The contribution of Coulomb electrostatic energy is a little bit larger (−8.2 kJ/mole, Figure 5a) as compared to dispersion energy (7.3 kJ/mole, Figure 5b). In the case of **DHBA**, the dispersion energy is far higher than the Coulomb electrostatic energy. The contribution of dispersion energy is −24.2 kJ/mole (Figure 5e), whereas the contribution of coulomb electrostatic energy is just −2.9 kJ/mole (Figure 5d). The total interaction energy is attractive for both compounds, but this energy is larger in **DHBA** as compared to **HMBA**.

### 2.3. Natural Population and Molecular Electrostatic Potential Analyses

A brief investigation on the atomic charges derived from natural bond orbitals (NBOs) of compounds **HMBA** and **DHBA** was presented in Figure S6. This approach provides a good input for obtaining information about the polarizability of molecules and electronic properties of the chemical systems [53]. The phenomenon associated with the charge transformation originating in reactions, the electrostatic potential on exteriors of crystal and the electronegativity equalization are frequently evaluated using this analysis [54]. The charges observed on atoms are considered as a substantial factor for bonding capacity as well as molecular conformation. The unequal electron density redistribution data, indicated by NBO charges, of studied compounds reveals the presence of highly electronegative elements such as nitrogen and oxygen [55]. Moreover, the MEP plot could be utilized to predict the chemical nature and reaction sites in the studied compounds [56,57]. Accompanying NPA, the MEP descriptor could be regarded as significant for understanding the EP surface activity and non-covalent interactions (NCIs) in the aforementioned compounds. The MEP surface distinguishes the reaction sites of any compound via various standard colors, such as orange, red, yellow, blue and green, to comprehensively explain the regions of electrophilic as well as nucleophilic attack. The charge contribution systematically declines in the order of red > orange > yellow > green > blue, where deep red specifies negative potential and deep blue represents positive potential [58]. In **HMBA** and **DHBA**, the electronic charges based on NPA and MEP heat maps were estimated by adopting M06 as a level of theory. NPA graphs of **HMBA** displayed (Figure S6) that some carbon and

most of the hydrogen atoms were positively charged, which was further supported by MEP maps (Figure S7) accomplished at the M06/6-31G(d,p) functional of DT-DFT, represented by a blue color. As the blue colored segment represents the nucleophile enticing site, it is assured to communicate with the most positive potential. Whereas, most of the C, N and O atoms were negatively charged, which is favorably prone to electrophilic attack as indicated by a red color (Figure S7). Similarly, for **DHBA**, iodine, sulfur, some of the carbons and most of the hydrogens were seen as positively charged. All the atoms were found positively charged, while oxygen, nitrogen and most of the carbons were negatively charged (See Figure S6); this was further supported by MEP maps with blue and red colors, respectively, as shown in Figure S7. Additionally, the plotted property  $d_{\text{norm}}$  of HS analysis also supported the NPA charges as the more electronegative regions (N, O and I) in HS are a red color, while electrophilic sites (C and H) are highlighted with blue and yellow colors (Figure 3). The development of NCI ( $S \cdots H/H \cdots S$  and  $O \cdots H/H \cdots O$ ) in molecules supported the NPA charges.

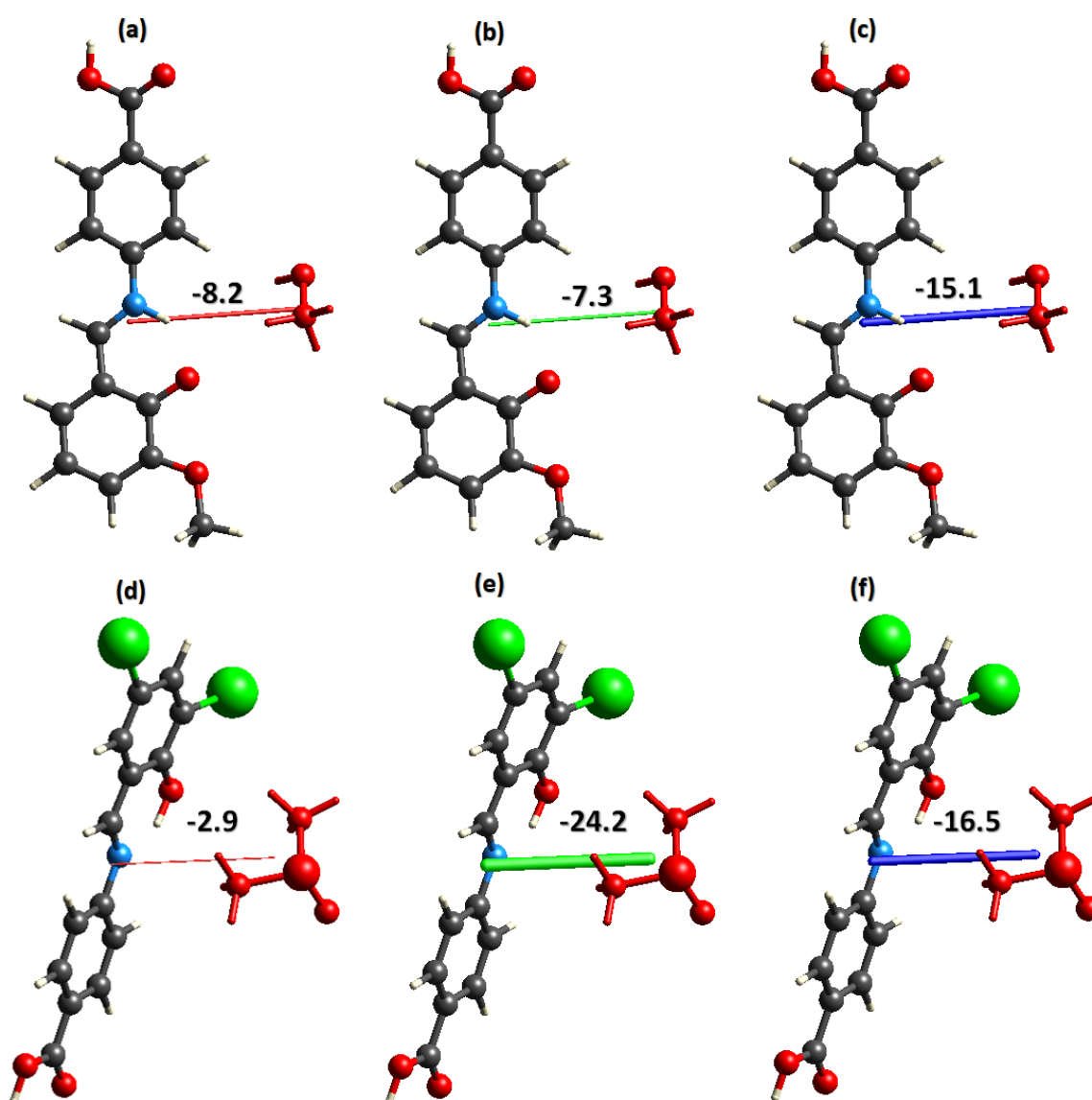


**Figure 5.** Coulomb, electrostatic, dispersive and total energy measured in kJ/mol (a–c) for **HMBA** and (d–f) **DHBA**.

#### 2.4. NBO Analysis

The NBO analysis provides a clear understanding regarding the molecular interactions, hyperconjugation and the charge transfer phenomena in the acceptor (Lewis acid) and donor (Lewis base) moieties [59,60]. Strong interactions between the donor and acceptor moieties harvest a large value for stabilization energy. The energy of stabilization  $E^{(2)}$  paired with the delocalization for every donor ( $i$ ) and acceptor ( $j$ ) moiety was estimated using Equation (1).

$$E^{(2)} = q_i \frac{(F_{i,j})^2}{\epsilon_j - \epsilon_i} \quad (1)$$

where  $E^{(2)}$  represents stabilization energy, the diagonal =  $F(i,j)$ , donor orbital occupancy =  $q_i$ , and the off-diagonal elements =  $\epsilon_i, \epsilon_j$  are NBO Fock matrix elements. Some important outcomes of NBOs for compounds **HMBA** and **DHBA** are listed in Table 2; meanwhile, Tables S6 and S7 demonstrated the rest of the transitions, representing established conjugation.

**Table 2.** Natural bond orbital (NBO) analysis of **HMBA** and **DHBA** compounds.

Compound	Donor ( $i$ )	Type	Acceptor ( $j$ )	Type	$E^{(2)}$ a [kcal/mol]	$E(j)-E(i)$ [a.u.]	$F(i,j)$ [a.u.]
<b>HMBA</b>	C8-H20	$\sigma$	C9-C10	$\sigma^*$	5.15	1.06	0.066
	C15-H31	$\sigma$	O4-C11	$\sigma^*$	0.55	0.92	0.02
	C4-C5	$\pi$	C2-C3	$\pi^*$	26.32	0.31	0.08
	C2-C3	$\pi$	C2-C3	$\pi^*$	0.61	0.3	0.012
	O2	LP(2)	O1-C1	$\pi^*$	47.09	0.37	0.121
	O1	LP(2)	O2-C1	$\sigma^*$	34.41	0.65	0.135
<b>DHBA</b>	C9-C10	$\sigma$	C10-C11	$\sigma^*$	6.42	1.26	0.08
	O3-H7	$\sigma$	N1-C5	$\sigma^*$	0.52	1.21	0.022
	C10-C11	$\pi$	C12-C13	$\pi^*$	30.68	0.3	0.086
	C9-C14	$\pi$	C9-C14	$\pi^*$	0.67	0.29	0.013
	O2	LP(2)	O1-C1	$\pi^*$	47.53	0.37	0.121
	O1	LP(2)	O2-C1	$\sigma^*$	34.35	0.65	0.135

The  $\sigma \rightarrow \sigma^*$ ,  $\pi \rightarrow \pi^*$ ,  $LP \rightarrow \sigma^*$  and  $LP \rightarrow \pi^*$  overlaps resulted in the intramolecular hyperconjugative interactions, which facilitated ICT, consequently resulting in the stability of the system. NBO analysis was performed for **HMBA** and **DHBA** at M06/6-311 G(d,p) functional. The comprehensive detail for NBO analysis of **HMBA** and **DHBA** was provided in Tables S6 and S7 and some typical values for **HMBA** and **DHBA** were presented in Table 2. In the studied compounds, the following transitions:  $\sigma \rightarrow \sigma^*$ ,  $\pi \rightarrow \pi^*$ ,  $LP \rightarrow \sigma^*$  and  $LP \rightarrow \pi^*$  are recognized. Among  $\sigma \rightarrow \sigma^*$ , important electronic transitions,  $\sigma$  (C8-H20)  $\rightarrow \sigma^*$  (C9-C10) and  $\sigma$  (C9-C10)  $\rightarrow \sigma^*$  (C10-C11) were spotted with the maximum stabilization energies, i.e., 5.15 and 6.42 kcal/mol for **HMBA** and **DHBA** compounds, respectively. Meanwhile, the transitions such as  $\sigma$  (C15-H31)  $\rightarrow \sigma^*$  (O4-C11) and  $\sigma$  (O3-H7)  $\rightarrow \sigma^*$  (N1-C5) were seen with the lowermost stabilization energies, i.e., 0.55 and 0.52 kcal/mol of **HMBA** and **DHBA** compounds, respectively. In case of compound **HMBA**,  $\pi \rightarrow \pi^*$  interactions such as  $\pi$  (C4-C5)  $\rightarrow \pi^*$  (C2-C3) having maximum stabilization energy values of 26.32 kcal/mol and  $\pi$  (C2-C3)  $\rightarrow \pi^*$  (C2-C3) having minimum stabilization energy value of 0.61 kcal/mol were seen. In compound **DHBA**, among  $\pi \rightarrow \pi^*$  transitions,  $\pi$  (C10-C11)  $\rightarrow \pi^*$  (C12-C13) and  $\pi$  (C9-C14)  $\rightarrow \pi^*$  (C9-C14) were significant transitions with maximum and minimum stabilization energies, i.e., 30.68 and 0.67 kcal/mol, respectively. Among  $LP \rightarrow \sigma^*$  transitions, LP2 (O1)  $\rightarrow \sigma^*$  (O2-C1) and LP2 (O1)  $\rightarrow \sigma^*$  (O2-C1) were found as the prominent transitions with the stabilization energies of 34.41 and 34.35 kcal/mol for **HMBA** and **DHBA** compounds, respectively. Meanwhile,  $LP \rightarrow \pi^*$  prominent transitions such as LP(2) (O2)  $\rightarrow \pi^*$  (O2-C1) and LP(2) (O2)  $\rightarrow \pi^*$  (O1-C1) were obtained with the stabilization energies of 47.09 and 47.53 kcal/mol for **HMBA** and **DHBA** compounds, respectively. The stability of

studied compounds was credited by good stabilization energies due to the phenomenon of resonance. The existence of hyperconjugation, extended conjugation and charge transfer were conclusively and precisely confirmed by the NBO data. However, the synergistic effect of charge transfer caused by extended conjugation leads to a significant red shifted behavior among the investigated compounds.

### 2.5. FMO Analysis

Through frontier molecular orbitals (FMOs) investigation, entitled compounds were not only analyzed for chemical stability but also interpreted for the optical as well as electronic responses [61,62]. HOMO to LUMO energy variation was considered to be responsible for the stability and reactivity of a compound. [63,64]. Furthermore, this energy difference ( $\Delta E = E_{LUMO} - E_{HOMO}$ ) was used for computing the various GRPs of the synthesized molecules (see Table 3). A greater chance of ICT was provided with a smaller energy gap among LUMO and HOMO orbitals and based on how effectively polarizable the molecule was and vice-versa [65,66]. The electronic properties of **HMBA** and **DHBA** compounds were determined by FMOs at the M06 level of TD-DFT. The energies of the first, second and third excited states of FMO orbitals were presented in Table 3.

**Table 3.** The orbital energies and their energy gaps of examined compounds; **HMBA** and **DHBA**, units are in eV.

MOs	HMBA		DHBA	
	<i>E</i>	$\Delta E$	<i>E</i>	$\Delta E$
HOMO	−5.894	3.477	−6.533	3.793
LUMO	−2.417		−2.740	
HOMO-1	−6.969	5.891	−6.924	5.181
LUMO+1	−1.078		−1.743	
HOMO-2	−7.567	6.917	−7.362	6.001
LUMO+2	−0.650		−1.361	

The band gaps of HOMO/LUMO in **HMBA** and **DHBA** compounds were found as 3.477 and 3.793 eV, respectively, with −5.894 and −6.533 eV. The energy gap noted in **DHBA** is higher as compared to **HMBA** which indicated it as more stable, and hard with little reactivity. The lower band gap in **HMBA** elucidated it as more reactive, less stable and softer than the former compound. This difference might originate from the presence of the electronegative iodine atom. In order to check the coherence in the energies, we calculated the energy level up to HOMO-2/LUMO+2. The  $E_{\text{gap}}$  of HOMO-1/LUMO+1 in **HMBA** and **DHBA** was observed as 5.891 and 5.181 eV, correspondingly. Likewise, the HOMO-2/LUMO+2 energy gap of **HMBA** and **DHBA** was noticed as 6.489 and 6.001 eV, respectively. Accompanying the energies of orbitals, the charge transference between the orbitals can also be estimated through FMOs study (see Figure 6). In the case of compound **HMBA**, in HOMO, the charge density was present on the part (Z)-2-methoxy-6-((methyl- $\lambda^2$ -azaneyl)methylene)cyclohexa-2,4-diene-1-one; whereas, in LUMO, the electronic cloud was dispersed over the entire compound. In addition, in **DHBA**, for HOMO, the charge density is primarily located on the dimethyl sulfoxide group of the crystal; whereas, in context of LUMO, it is condensed on the complete molecule. For HOMO-1/LUMO+1 and HOMO-2/LUMO+2, the electron density is located over the molecule in **HMBA**. Similarly, a trend is seen for **DHBA** in the case of HOMO-2/LUMO+2, while for HOMO-1/LUMO+1, the electronic cloud is located at (Z)-2-methoxy-6-((methyl- $\lambda^2$ -azaneyl)methylene)cyclohexa-2,4-diene-1-one.

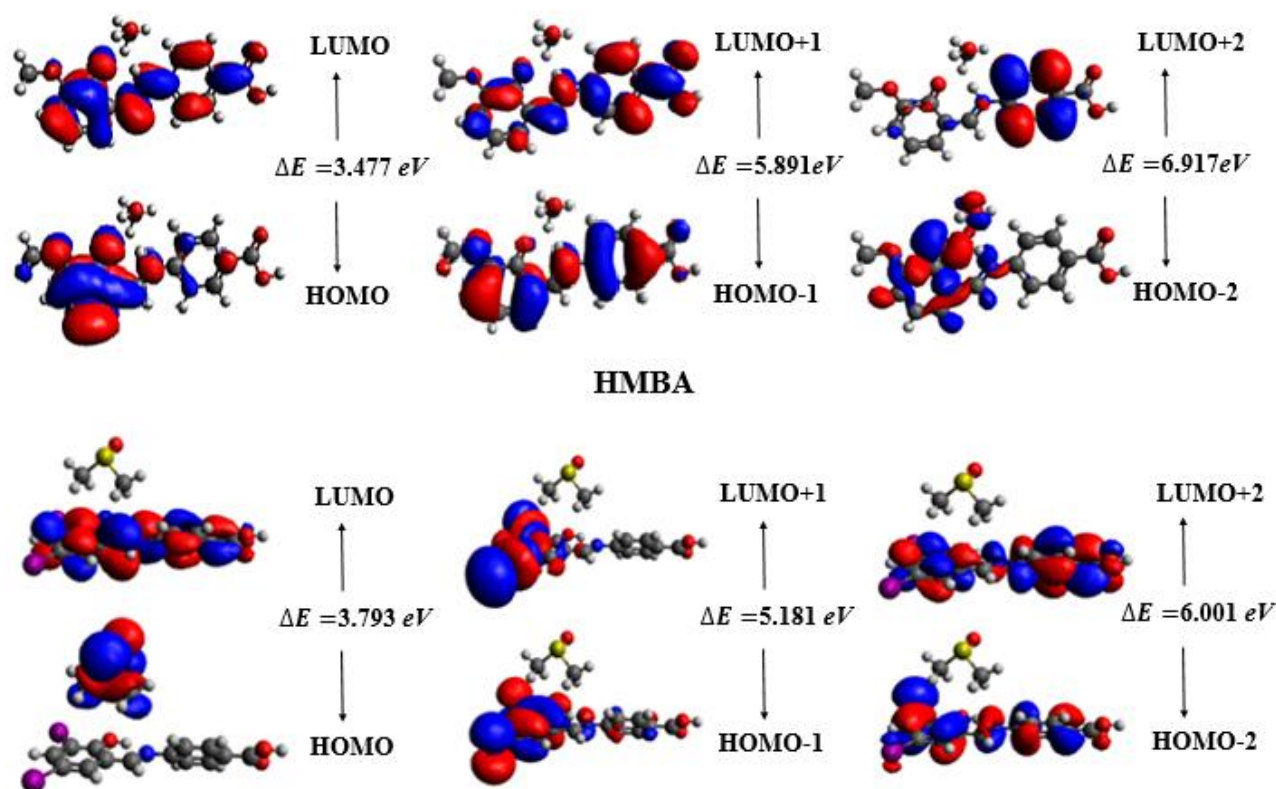


Figure 6. Frontier molecular orbitals HMBA and DHBA compounds.

### 2.6. Global Reactivity Parameters

The electronegativity ( $X$ ) [67], electron affinity ( $A$ ), ionization potential ( $I$ ) [68], global electrophilicity index ( $\omega$ ) [69], global softness ( $\sigma$ ) [70], chemical potential ( $\mu$ ) [71] and global hardness ( $\eta$ ) [72] were calculated by utilizing the energies of FMOs. The GRPs of **HMBA** and **DHBA** compounds are estimated by utilizing Equations (2)–(7) and outcomes are illustrated in Table 4.

Table 4. Global reactivity parameters of HMBA and DHBA.

Compounds	$I$	$A$	$X$	$\eta$	$\mu$	$\omega$	$\sigma$
<b>HMBA</b>	5.894	2.417	4.155	1.738	−4.155	4.966	3.484
<b>DHBA</b>	6.533	2.740	4.636	1.896	−4.636	5.667	3.802

All units are in eV while softness is in  $\text{eV}^{-1}$ .

The major findings obtained via Equations (6)–(11) were shown in Table 4. Thus, the electron withdrawing and donating capabilities of the aforementioned compounds were depicted by  $I$  and  $A$ . In the aforementioned compounds, the values of  $I$  and  $A$  were found higher in **DHBA** as compared to **HMBA**, which showed that **DHBA** had a greater ability to accept the electron than **HMBA**. Moreover, the electronegativity values were found to be [**DHBA** ( $X = 4.636 \text{ eV}$ )] > [**HMBA** ( $X = 4.155 \text{ eV}$ )]. The global electrophilicity ( $\omega$ ) trend for **HMBA** and **DHBA** was 4.966 and 5.667 eV, respectively. The reactivity as well stability of the studied chromophores are indicated by the parameters such as global softness ( $\sigma$ ) and global hardness ( $\eta$ ) of the studied compounds. The molecules possessing a smaller band gap could be considered as soft, chemically reactive and unstable. Contrarily, compounds with a larger band gap can be categorized as hard, less reactive and kinetically stable candidates. Table 4 showed that the compound **HMBA** had a higher global softness value ( $\sigma = 3.484 \text{ eV}^{-1}$ ) than **DHBA** ( $\sigma = 3.802 \text{ eV}^{-1}$ ). Similarly, the value of global hardness for **DHBA** was higher than **HMBA**, i.e., 5.667 and 4.966, respectively. All the global reactivity

parameters collectively disclosed that **HMBA** was a softer and more reactive compound than **DHBA** (Table 4).

### 2.7. Dipole Moment and Linear Polarizability

Inorganic and organic materials are regarded as effective optical materials because of their significant contributions in optical logic for advanced technologies such as signal modulation and telecommunications [73,74]. The intra-molecular charge transfer and larger conjugation of electrons in organic chromophores have expanded their roles as opto-electronic materials as compared to inorganic compounds [68–75]. The values of dipole moment ( $\mu$ ) and linear polarizability  $\langle\alpha\rangle$  for studied chromophores were computed by applying M06 level of theory; the results were tabulated in Table S8. Urea is the reference compound most commonly exploited in the examination of the opto-electronic response of various molecules, and is considered as a threshold standard for comparing the  $\langle\alpha\rangle$  response of studied molecules [76]. **HMBA** and **DHBA** are regarded as polar molecules as they comprise non-zero dipole moments 6.34 and 5.76 D, respectively. The higher contribution among all the axes is seen along the y axis:  $\mu_y = -5.55$  and 5.68 D in **HMBA** and **DHBA**, respectively. The values of dipole moment calculated for the studied molecules are found to be greater as compared to urea (1.37 D) [77]. The computed average polarizabilities  $\langle\alpha\rangle$  of **HMBA** and **DHBA** were found out to be 313.48 and 288.79 a.u, respectively. Among explored molecules, the average polarizability value of **HMBA** is greater compared to **DHBA**. These values of average polarizability  $\langle\alpha\rangle$  of **HMBA** and **DHBA** are found to be 11.34 and 10.45 times larger than standard molecule urea ( $\langle\alpha\rangle = 27.63$ ) [25]. The major contribution tensor is examined along the x-axis  $\alpha_{xx} = 528.79$  and 436.95 a.u, for **HMBA** and **DHBA**, respectively, among all the tensors.

## 3. Methodology

### 3.1. Experimental Details

The carboxylic acid functionalized imines compounds were synthesized utilizing 4-aminobenzoic acid and substituted benzaldehydes of maximum purity, as they were purchased and used without further purification. The standard chemicals were purchased from the reputed chemical suppliers such as Sigma-Aldrich, Macklin, Acros Chemicals, BDH and TCI. Solvent purification was accomplished by a simple distillation procedure. Thin-layer chromatography (TLC) employing the aluminum sheet priorly coated with silica gel was utilized for the reaction progress. For the SC-XRD study, a Bruker Kappa Apex-II diffractometer was utilized with an X-ray source producing Mo-K $\alpha$  radiations. Software Apex-II [78], SAINT [79], SHEXS-97 [80] and SHEXL 2018/3 [81] were used for the sake of collecting data, integrating data, making a structure solution from raw data, and for refining data, respectively. All the H-atoms of **HMBA** and **DHBA** were assigned relative isotropic displacement parameters except the H-atom attached to N1 and O2 of **HMBA** which were refined independently by keen investigation of the remaining electron density peaks. The SC-XRD findings were graphically represented by PLATON [82], Mercury 4.0 [83] and ORTEP-3 [84] software.

### 3.2. Synthesis of the Carboxylic Acid Functionalized Imines

The carboxylic acid functionalized imines compounds **HMBA** and **DHBA** were produced by the condensation reaction strategy using 4-aminobenzoic acid and substituted benzaldehyde.

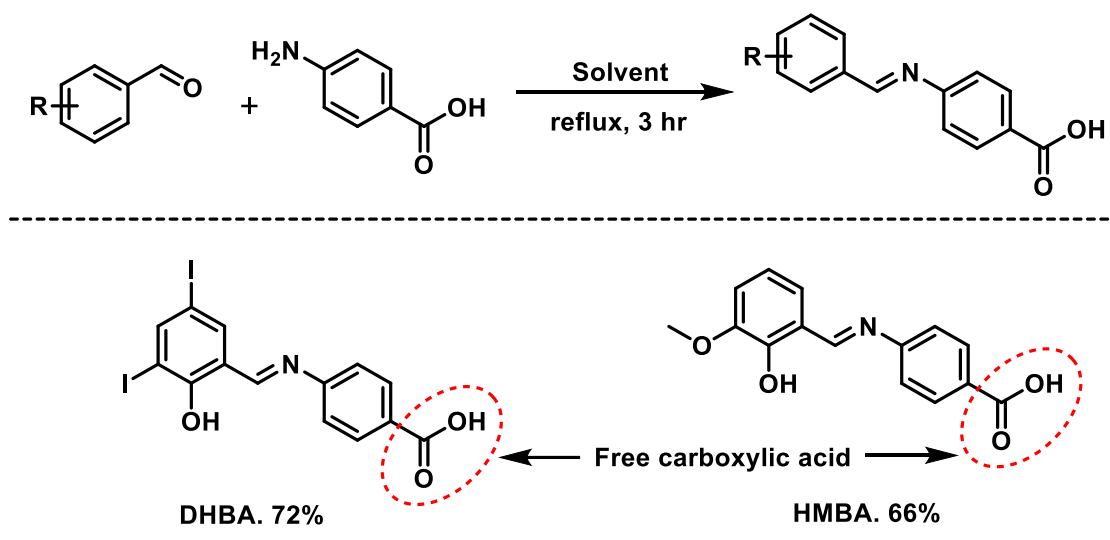
#### 3.2.1. Synthesis of (E)-4-((3,5-Diiodo-2-Hydroxybenzylidene)Amino)Benzoic Acid (DHBA)

In a round bottom flask (50 mL), we had 3,5-diiodo-2-hydroxybenzaldehyde (1 mmol) in 30 mL methanol to which we added 4-aminobenzoic acid (1.2 mmol) and the reaction mixture was subjected to reflux conditions for 3 h. After completing the reaction (guessed by TLC), methanol was removed under lower pressure and then an aqueous workup of the mixture was performed. The dry organic layer was reduced using a rotary evaporator. The

compound was purified using column chromatography and recrystallized for the SC-XRD analysis.

### 3.2.2. Synthesis of (E)-4-((2-Hydroxy-3-Methoxybenzylidene)Amino)Benzoic Acid (HMBA)

The synthesis of chromophore **HMBA** was also carried out by utilizing the same procedure as above, except using 2-hydroxy-3-methoxybenzaldehyde as the aldehyde component and methanol as the solvent, see Scheme 1.



**Scheme 1.** Synthesis of aminobenzoic acid based crystalline imines **HMBA** and **DHBA**.

### 3.3. Computational Procedure

In the current study, all the DFT calculations for aminobenzoic acid-based compounds (**HMBA** and **DHBA**) were accomplished through the Gaussian 09 program [85] at M06/6-311G(d,p) functional [86]. From the literature, we found that M06/6-31G (d,p) is highly parameterized to approximate exchange-correlation energy functionals in DFT, utilized significantly for calculations of excited states, non-covalent interactions and bonding phenomena; therefore, we utilized M06 functional for this investigation [86,87]. At first, optimizations of geometries were performed, and confirmation of the true minima was determined by the lack of negative frequencies. Various kinds of analyses, NBO, NPA, dipole moment and linear polarizability analyses were performed by utilizing the optimized geometries of **HMBA** and **DHBA** in the gaseous phase. For the NBO investigation, NBO software package 3.1 [88] was utilized. Time-dependent density functional theory (TDDFT) was used to calculate the FMOs, and MEP-based findings. To understand the reactivity of the aforementioned compounds, GRPs were determined by utilizing energies of HOMO/LUMOs with the aid of Equations (2)–(7).

$$I = -E_{\text{HOMO}} \quad (2)$$

$$A = -E_{\text{LUMO}} \quad (3)$$

$$\eta = \frac{I - A}{2} \quad (4)$$

$$X = \frac{I + A}{2} \quad (5)$$

$$\omega = \frac{\mu^2}{\eta} \quad (6)$$

$$\sigma = \frac{1}{2\eta} \quad (7)$$

Different types of software such as Gauss View 5.0 [89], Gauss Sum [90], Chemcraft [91] and Avogadro [92] had been utilized for the interpretation of data from outputs.

#### 4. Conclusions

The synthesis of two carboxylic acid functionalized imines compounds **DHBA** and **HMBA** has been accomplished in reasonable yields and characterized by SC-XRD analysis. This study specifies the effect of intramolecular interaction in the stabilization of the molecular configuration of both compounds and the roles of strong and weak NCIs in the packing of the crystals. The intermolecular interactions of strong and weak natures are explored and compared by Hirshfeld surface analysis. The synthesized crystals are computed for their electronic, structural and comparative analyses. The NBO study depicted that the intramolecular H-bonding and some prominent transitions  $LP2(O1) \rightarrow \sigma^*(O2-C1)$  and  $LP2(O1) \rightarrow \sigma^*(O2-C1)$  with the highest energy of stabilization of 34.41 and 34.35 kcal/mol for **HMBA** and **DHBA**, respectively, exist in both synthesized compounds, and this played an important role in stabilizing the compounds. The FMOs analysis revealed that the band gap (3.477 eV) of **HMBA** is comparatively smaller than that of **DHBA** (3.793 eV), which shows higher polarizability in **HMBA**. The comparative study with urea indicated that both molecules exhibited significant behaviors of linear responses and can be used as efficient opto-electronic materials.

**X-ray Crystallography:** Deposition Numbers 2117442 for **HMBA** and 2117443 for **DHBA** contain the supplementary crystallographic data for this paper. These data are provided free of charge by the joint Cambridge Crystallographic Data Centre and Fachinformationszentrum Karlsruhe Access Structures service.

**Supplementary Materials:** The following supporting information can be downloaded at: <https://www.mdpi.com/article/10.3390/molecules28072967/s1>, SC-XRD, comparison between XRD and DFT values, enrichment ratio of pair of chemical species, NBO data, dipole moment, polarizability, MEP maps of synthesized compounds.

**Author Contributions:** Conceptualization: A.A. and M.K.; Methodology: M.K., S.M. and I.S.; Software: M.K. and I.S.; Validation: I.S.; Formal analysis: M.A., M.N. and M.A.A.; Investigation: M.A., I.S., M.A.A. and S.P.; Resources: M.N.T. and A.A.; Data curation: M.N.T., M.A., M.N., M.A.A. and R.O.; Writing-original draft: M.A., M.N., I.S., R.O. and S.P.; Writing-review & editing: M.N.T., S.M. All authors have read and agreed to the published version of the manuscript.

**Funding:** The authors extend their appreciation to the Researcher Supporting Project number (RSP2023R431), King Saud University, Riyadh, Saudi Arabia, for funding this research work.

**Institutional Review Board Statement:** Not applicable.

**Informed Consent Statement:** Not applicable.

**Data Availability Statement:** The experimental details including computational details are given in the supporting information.

**Acknowledgments:** The authors extend their appreciation to the Researcher Supporting Project number (RSP2023R431), King Saud University, Riyadh, Saudi Arabia, for funding this research work. Moreover, Muhammad Khalid gratefully acknowledges the financial support of HEC Pakistan (project no. 20 14703/NRPU/R&D/HEC/2021).

**Conflicts of Interest:** The authors declare no competing financial interest.

**Sample Availability:** Samples of the compounds are available from the authors.

## References

1. Cimerman, Z.; Miljanić, S.; Galić, N. Schiff Bases Derived from Aminopyridines as Spectrofluorimetric Analytical Reagents. *Croat. Chem. Acta* **2000**, *73*, 81–95.
2. Abu-Dief, A.M.; Mohamed, I.M. A Review on Versatile Applications of Transition Metal Complexes Incorporating Schiff Bases. *Beni-Suef Univ. J. Basic Appl. Sci.* **2015**, *4*, 119–133. [[CrossRef](#)]
3. Malik, A.N.; Kuznetsov, A.; Ali, A.; Ashfaq, M.; Tahir, M.N.; Siddique, A. Imine-Based Zwitterion: Synthesis, Single-Crystal Characterization, and Computational Investigation. *J. Mol. Struct.* **2022**, *1253*, 132237. [[CrossRef](#)]
4. Kajal, A.; Bala, S.; Kamboj, S.; Sharma, N.; Saini, V. Schiff Bases: A Versatile Pharmacophore. *J. Catal.* **2013**, *2013*, 893512. [[CrossRef](#)]
5. Ali, S.M.M.; Azad, M.A.K.; Jesmin, M.; Ahsan, S.; Rahman, M.M.; Khanam, J.A.; Islam, M.N.; Shahriar, S.M.S. In Vivo Anticancer Activity of Vanillin Semicarbazone. *Asian Pac. J. Trop. Biomed.* **2012**, *2*, 438–442. [[CrossRef](#)] [[PubMed](#)]
6. Aboul-Fadl, T.; Mohammed, F.A.-H.; Hassan, E.A.-S. Synthesis, Antitubercular Activity and Pharmacokinetic Studies of Some Schiff Bases Derived from 1-Alkylisatin and Isonicotinic Acid Hydrazide (INH). *Arch. Pharm. Res.* **2003**, *26*, 778–784. [[CrossRef](#)]
7. Sondhi, S.M.; Singh, N.; Kumar, A.; Lozach, O.; Meijer, L. Synthesis, Anti-Inflammatory, Analgesic and Kinase (CDK-1, CDK-5 and GSK-3) Inhibition Activity Evaluation of Benzimidazole/Benzoxazole Derivatives and Some Schiff's Bases. *Bioorg. Med. Chem.* **2006**, *14*, 3758–3765. [[CrossRef](#)]
8. Mounika, K.; Pragathi, A.; Gyanakumari, C. Synthesis Characterization and Biological Activity of a Schiff Base Derived from 3-Ethoxy Salicylaldehyde and 2-Amino Benzoic Acid and Its Transition Metal Complexes. *J. Sci. Res.* **2010**, *2*, 513. [[CrossRef](#)]
9. Majumdar, D.; Das, D.; Nag, S.; Bhattacharyya, M.; Singh, D.K.; Parai, D.; Bankura, K.; Mishra, D. A Rare Hetero-Bimetallic Zn (II)/Ca (II) Schiff Base Complex: Synthesis, Crystal Structure, DFT, Molecular Docking and Unveiling Antimicrobial Activity. *J. Mol. Struct.* **2020**, *1222*, 128951. [[CrossRef](#)]
10. Wei, D.; Li, N.; Lu, G.; Yao, K. Synthesis, Catalytic and Biological Activity of Novel Dinuclear Copper Complex with Schiff Base. *Sci. China Ser. B* **2006**, *49*, 225–229. [[CrossRef](#)]
11. Mahmood, A.; Saqib, M.; Ali, M.; Abdullah, M.I.; Khalid, B. Theoretical Investigation for the Designing of Novel Antioxidants. *Can. J. Chem.* **2013**, *91*, 126–130. [[CrossRef](#)]
12. Avaji, P.G.; Kumar, C.V.; Patil, S.A.; Shivananda, K.N.; Nagaraju, C. Synthesis, Spectral Characterization, in-Vitro Microbiological Evaluation and Cytotoxic Activities of Novel Macrocylic Bis Hydrazone. *Eur. J. Med. Chem.* **2009**, *44*, 3552–3559. [[CrossRef](#)] [[PubMed](#)]
13. Wang, Y.-F.; Wang, C.-J.; Feng, Q.-Z.; Zhai, J.-J.; Qi, S.-S.; Zhong, A.-G.; Chu, M.-M.; Xu, D.-Q. Copper-Catalyzed Asymmetric 1, 6-Conjugate Addition of in Situ Generated Para-Quinone Methides with  $\beta$ -Ketoesters. *Chem. Commun.* **2022**, *58*, 6653–6656. [[CrossRef](#)]
14. Yao, W.; Wang, J.; Zhong, A.; Wang, S.; Shao, Y. Transition-Metal-Free Catalytic Hydroboration Reduction of Amides to Amines. *Org. Chem. Front.* **2020**, *7*, 3515–3520. [[CrossRef](#)]
15. Yao, W.; Fang, H.; He, Q.; Peng, D.; Liu, G.; Huang, Z. A  $\text{BeEt}_3$ -Base Catalyst for Amide Reduction with Silane. *J. Org. Chem.* **2019**, *84*, 6084–6093. [[CrossRef](#)] [[PubMed](#)]
16. Chaubey, A.K.; Pandeya, S.N. Synthesis & Anticonvulsant Activity (Chemo Shock) of Schiff and Mannich Bases of Isatin Derivatives with 2-Amino Pyridine (Mechanism of Action). *Int. J. PharmTech Res.* **2012**, *4*, 590–598.
17. Yao, W.; He, L.; Han, D.; Zhong, A. Sodium Triethylborohydride-Catalyzed Controlled Reduction of Unactivated Amides to Secondary or Tertiary Amines. *J. Org. Chem.* **2019**, *84*, 14627–14635. [[CrossRef](#)]
18. Tamer, Ö.; Dege, N.; Demirtaş, G.; Avcı, D.; Atalay, Y.; Macit, M.; Şahin, S. Crystal Structure and Spectroscopic Characterization of (E)-2-(((4-Bromo-2-(Trifluoromethoxy) Phenyl) Imino) Methyl)-4-Nitrophenol: A Combined Experimental and Computational Study. *J. Mol. Struct.* **2014**, *1063*, 295–306. [[CrossRef](#)]
19. Kanmazalp, S.D.; Macit, M.; Dege, N. Hirshfeld Surface, Crystal Structure and Spectroscopic Characterization of (E)-4-(Diethylamino)-2-((4-Phenoxyphenylimino) Methyl) Phenol with DFT Studies. *J. Mol. Struct.* **2019**, *1179*, 181–191. [[CrossRef](#)]
20. Erkkilä, A.; Majander, I.; Pihko, P.M. Iminium Catalysis. *Chem. Rev.* **2007**, *107*, 5416–5470. [[CrossRef](#)] [[PubMed](#)]
21. Martin, S.F. Recent Applications of Imines as Key Intermediates in the Synthesis of Alkaloids and Novel Nitrogen Heterocycles. *Pure Appl. Chem.* **2009**, *81*, 195–204. [[CrossRef](#)]
22. de la Torre, A.F.; Ali, A.; Galetto, F.Z.; Braga, A.L.; Delgado, J.A.; Paixão, M.W. One-Pot Organocatalytic/Multicomponent Approach for the Preparation of Novel Enantioenriched Non-Natural Selenium-Based Peptoids and Peptide–Peptoid Conjugates. *Mol. Divers.* **2020**, *24*, 1–10. [[CrossRef](#)]
23. Alexander, F.; Ali, A.; Concepcion, O.; Montero-Alejo, A.L.; Muñoz, F.M.; Jiménez, C.A.; Belmar, J.; Velázquez-Libera, J.L.; Hernández-Rodríguez, E.W.; Caballero, J. A Study of the Cis–Trans Isomerization Preference of N-Alkylated Peptides Containing Phosphorus in the Side Chain and Backbone. *New J. Chem.* **2019**, *43*, 12804–12813. [[CrossRef](#)]
24. Berge, S.M.; Bighley, L.D.; Monkhouse, D.C. Pharmaceutical Salts. *J. Pharm. Sci.* **1977**, *66*, 1–19. [[CrossRef](#)]
25. Khan, I.; Khalid, M.; Adeel, M.; Niaz, S.I.; Shafiq, I.; Muhammad, S.; Braga, A.A.C. Palladium-Catalyzed Synthesis of 5-(Arylated) Pyrimidines, Their Characterization, Electronic Communication, and Non-Linear Optical Evaluations. *J. Mol. Struct.* **2021**, *1237*, 130408. [[CrossRef](#)]
26. Badea, G.-I.; Radu, G.L. *Carboxylic Acid: Key Role in Life Sciences*; BoD—Books on Demand: Norderstedt, Germany, 2018.

27. Tamer, Ö.; Mahmood, H.; Feyzioglu, K.F.; Kilinc, O.; Avci, D.; Orun, O.; Dege, N.; Atalay, Y. Synthesis of the First Mixed Ligand Mn (II) and Cd (II) Complexes of 4-Methoxy-Pyridine-2-Carboxylic Acid, Molecular Docking Studies and Investigation of Their Anti-Tumor Effects in Vitro. *Appl. Organomet. Chem.* **2020**, *34*, e5416. [[CrossRef](#)]
28. Avci, D.; Altürk, S.; Sönmez, F.; Tamer, Ö.; Başoğlu, A.; Atalay, Y.; Zengin Kurt, B.; Dege, N. Novel Metal Complexes Containing 6-Methylpyridine-2-Carboxylic Acid as Potent  $\alpha$ -Glucosidase Inhibitor: Synthesis, Crystal Structures, DFT Calculations, and Molecular Docking. *Mol. Divers.* **2021**, *25*, 171–189. [[CrossRef](#)]
29. Avci, D.; Saeedi, Y.; Başoğlu, A.; Dege, N.; Altürk, S.; Tamer, Ö.; Atalay, Y. Novel Mn (II) and Zn (II) Complexes of 6-Bromopicolinic Acid as a Potential Optical Material: Synthesis, Spectral Characterizations, Linear, and Nonlinear Optical Properties and Density Functional Theory Calculations. *Appl. Organomet. Chem.* **2021**, *35*, e6125. [[CrossRef](#)]
30. Ali, A.; Khalid, M.; Rehman, M.F.U.; Haq, S.; Ali, A.; Tahir, M.N.; Ashfaq, M.; Rasool, F.; Braga, A.A.C. Efficient Synthesis, SC-XRD, and Theoretical Studies of O-Benzenesulfonylated Pyrimidines: Role of Noncovalent Interaction Influence in Their Supramolecular Network. *ACS Omega* **2020**, *5*, 15115–15128. [[CrossRef](#)] [[PubMed](#)]
31. Khalid, M.; Ali, A.; Abid, S.; Tahir, M.N.; Khan, M.U.; Ashfaq, M.; Imran, M.; Ahmad, A. Facile Ultrasound-Based Synthesis, SC-XRD, DFT Exploration of the Substituted Acyl-Hydrazones: An Experimental and Theoretical Slant towards Supramolecular Chemistry. *ChemistrySelect* **2020**, *5*, 14844–14856. [[CrossRef](#)]
32. Khalid, M.; Ali, A.; De la Torre, A.F.; Marrugo, K.P.; Concepcion, O.; Kamal, G.M.; Muhammad, S.; Al-Sehemi, A.G. Facile Synthesis, Spectral (IR, Mass, UV-Vis, NMR), Linear and Nonlinear Investigation of the Novel Phosphonate Compounds: A Combined Experimental and Simulation Study. *ChemistrySelect* **2020**, *5*, 2994–3006. [[CrossRef](#)]
33. Ali, A.; Khalid, M.; Marrugo, K.P.; Kamal, G.M.; Saleem, M.; Khan, M.U.; Concepción, O.; Alexander, F. Spectroscopic and DFT/TDDFT Insights of the Novel Phosphonate Imine Compounds. *J. Mol. Struct.* **2020**, *1207*, 127838. [[CrossRef](#)]
34. Amin, S.; Sher, M.; Ali, A.; Rehman, M.F.; Hayat, A.; Ikram, M.; Abbas, A.; Amin, H.M. Sulfonamide-Functionalized Silver Nanoparticles as an Analytical Nanoprobe for Selective Ni (II) Sensing with Synergistic Antimicrobial Activity. *Environ. Nanotechnol. Monit. Manag.* **2022**, *18*, 100735. [[CrossRef](#)]
35. Siddiqui, W.A.; Khalid, M.; Ashraf, A.; Shafiq, I.; Parvez, M.; Imran, M.; Irfan, A.; Hanif, M.; Khan, M.U.; Sher, F.; et al. Antibacterial Metal Complexes of O-Sulfamoylbenzoic Acid: Synthesis, Characterization, and DFT Study. *Appl. Organomet. Chem.* **2022**, *36*, e6464. [[CrossRef](#)]
36. Bernstein, J.; Davis, R.E.; Shimoni, L.; Chang, N.-L. Patterns in Hydrogen Bonding: Functionality and Graph Set Analysis in Crystals. *Angew. Chem. Int. Ed. Engl.* **1995**, *34*, 1555–1573. [[CrossRef](#)]
37. Bürgi, H.B.; Dunitz, J.D. Crystal and Molecular Structures of Benzylideneaniline, Benzylideneaniline-p-Carboxylic Acid and p-Methylbenzylidene-p-Nitroaniline. *Helv. Chim. Acta* **1970**, *53*, 1747–1764. [[CrossRef](#)]
38. Harada, J.; Harakawa, M.; Ogawa, K. Torsional Vibration and Central Bond Length of N-Benzylideneanilines. *Acta Crystallogr. B* **2004**, *60*, 578–588. [[CrossRef](#)] [[PubMed](#)]
39. Akkurt, M.; Yıldırım, S.Ö.; Asiri, A.M.; McKee, V. 4-[(2-Hydroxy-1-Naphthyl) Methylideneamino] Benzoic Acid. *Acta Crystallogr. Sect. E Struct. Rep. Online* **2008**, *64*, o682. [[CrossRef](#)]
40. Johmoto, K.; Ishida, T.; Sekine, A.; Uekusa, H.; Ohashi, Y. Relation between Photochromic Properties and Molecular Structures in Salicylideneaniline Crystals. *Acta Crystallogr. B* **2012**, *68*, 297–304. [[CrossRef](#)]
41. Johmoto, K.; Sekine, A.; Uekusa, H. Photochromism Control of Salicylideneaniline Derivatives by Acid–Base Co-Crystallization. *Cryst. Growth Des.* **2012**, *12*, 4779–4786. [[CrossRef](#)]
42. Han, T.; Wei, W.; Yuan, J.; Duan, Y.; Li, Y.; Hu, L.; Dong, Y. Solvent-Assisted Self-Assembly of an AIE+ TICT Fluorescent Schiff Base for the Improved Ammonia Detection. *Talanta* **2016**, *150*, 104–112. [[CrossRef](#)]
43. Spackman, P.R.; Turner, M.J.; McKinnon, J.J.; Wolff, S.K.; Grimwood, D.J.; Jayatilaka, D.; Spackman, M.A. CrystalExplorer: A Program for Hirshfeld Surface Analysis, Visualization and Quantitative Analysis of Molecular Crystals. *J. Appl. Crystallogr.* **2021**, *54*, 1006–1011. [[CrossRef](#)]
44. Spackman, M.A.; Jayatilaka, D. Hirshfeld Surface Analysis. *CrystEngComm* **2009**, *11*, 19–32. [[CrossRef](#)]
45. Madni, M.; Ahmed, M.N.; Hafeez, M.; Ashfaq, M.; Tahir, M.N.; Gil, D.M.; Galmés, B.; Hameed, S.; Frontera, A. Recurrent  $\pi$ – $\pi$  Stacking Motifs in Three New 4,5-Dihydropyrazolyl–Thiazole–Coumarin Hybrids: X-ray Characterization, Hirshfeld Surface Analysis and DFT Calculations. *New J. Chem.* **2020**, *44*, 14592–14603. [[CrossRef](#)]
46. Khalid, M.; Ali, A.; Tariq, J.; Tahir, M.N.; Aliabad, H.A.R.; Hussain, I.; Ashfaq, M.; Khan, M.U. Stabilization of Supramolecular Assembly of N-Substituted Benzylidene Acetohydrazide Analogs by Non-Covalent Interactions: A Concise Experimental and Theoretical Approach. *ChemistrySelect* **2020**, *5*, 10618–10631. [[CrossRef](#)]
47. Ashfaq, M.; Bogdanov, G.; Glebov, V.; Ali, A.; Tahir, M.N.; Abdullah, S. Single Crystal Investigation, Hirshfeld Surface Analysis and DFT Exploration of the Pyrimethamine-Based Novel Organic Salt: 2,4-Diamino-5-(4-Chlorophenyl)-6-Ethylpyrimidin-1-ium 3-Carboxybenzoate Hydrate (1:1:1). *J. Mol. Struct.* **2021**, *1224*, 129309. [[CrossRef](#)]
48. Ashfaq, M.; Ali, A.; Kuznetsov, A.; Tahir, M.N.; Khalid, M. DFT and Single-Crystal Investigation of the Pyrimethamine-Based Novel Co-Crystal Salt: 2,4-Diamino-5-(4-Chlorophenyl)-6-Ethylpyrimidin-1-ium-4-Methylbenzoate Hydrate (1:1:1)(DEMH). *J. Mol. Struct.* **2021**, *1228*, 129445. [[CrossRef](#)]
49. Ashfaq, M.; Munawar, K.S.; Tahir, M.N.; Dege, N.; Yaman, M.; Muhammad, S.; Alarfaji, S.S.; Kargar, H.; Arshad, M.U. Synthesis, Crystal Structure, Hirshfeld Surface Analysis, and Computational Study of a Novel Organic Salt Obtained from Benzylamine and an Acidic Component. *ACS Omega* **2021**, *6*, 22357–22366. [[CrossRef](#)] [[PubMed](#)]

50. Jelsch, C.; Ejsmont, K.; Huder, L. The Enrichment Ratio of Atomic Contacts in Crystals, an Indicator Derived from the Hirshfeld Surface Analysis. *IUCr* **2014**, *1*, 119–128. [[CrossRef](#)]
51. Turner, M.J.; McKinnon, J.J.; Jayatilaka, D.; Spackman, M.A. Visualisation and Characterisation of Voids in Crystalline Materials. *CrystEngComm* **2011**, *13*, 1804–1813. [[CrossRef](#)]
52. Khan, B.A.; Hamdani, S.S.; Ahmed, M.N.; Hameed, S.; Ashfaq, M.; Shawky, A.M.; Ibrahim, M.A.; Sidhom, P.A. Synthesis, X-Ray Diffraction Analysis, Quantum Chemical Studies and  $\alpha$ -Amylase Inhibition of Probenecid Derived S-Alkylphthalimide-Oxadiazole-Benzenesulfonamide Hybrids. *J. Enzyme Inhib. Med. Chem.* **2022**, *37*, 1464–1478. [[CrossRef](#)]
53. Khosravi, I.; Hosseini, F.; Khorshidifard, M.; Sahihi, M.; Rudbari, H.A. Synthesis, Characterization, Crystal Structure and HSA Binding of Two New N, O, O-Donor Schiff-Base Ligands Derived from Dihydroxybenzaldehyde and Tert-Butylamine. *J. Mol. Struct.* **2016**, *1119*, 373–384. [[CrossRef](#)]
54. Mulliken, R.S. Electronic Population Analysis on LCAO–MO Molecular Wave Functions. I. *J. Chem. Phys.* **1955**, *23*, 1833–1840. [[CrossRef](#)]
55. Li, L.; Wu, C.; Wang, Z.; Zhao, L.; Li, Z.; Sun, C.; Sun, T. Density Functional Theory (DFT) and Natural Bond Orbital (NBO) Study of Vibrational Spectra and Intramolecular Hydrogen Bond Interaction of L-Ornithine–L-Aspartate. *Spectrochim. Acta. A Mol. Biomol. Spectrosc.* **2015**, *136*, 338–346. [[CrossRef](#)] [[PubMed](#)]
56. Zhao, D.; Liu, S.; Rong, C.; Zhong, A.; Liu, S. Toward Understanding the Isomeric Stability of Fullerenes with Density Functional Theory and the Information-Theoretic Approach. *ACS Omega* **2018**, *3*, 17986–17990. [[CrossRef](#)] [[PubMed](#)]
57. Cao, X.; Rong, C.; Zhong, A.; Lu, T.; Liu, S. Molecular Acidity: An Accurate Description with Information-Theoretic Approach in Density Functional Reactivity Theory. *J. Comput. Chem.* **2018**, *39*, 117–129. [[CrossRef](#)]
58. Khalid, M.; Ali, A.; Khan, M.U.; Tahir, M.N.; Ahmad, A.; Ashfaq, M.; Hussain, R.; de Alcantara Morais, S.F.; Braga, A.A.C. Non-Covalent Interactions Abetted Supramolecular Arrangements of N-Substituted Benzylidene Acetohydrazide to Direct Its Solid-State Network. *J. Mol. Struct.* **2021**, *1230*, 129827. [[CrossRef](#)]
59. James, C.; Raj, A.A.; Reghunathan, R.; Jayakumar, V.S.; Joe, I.H. Structural Conformation and Vibrational Spectroscopic Studies of 2, 6-Bis (p-N, N-Dimethyl Benzylidene) Cyclohexanone Using Density Functional Theory. *J. Raman Spectrosc. Int. J. Orig. Work Asp. Raman Spectrosc. High. Order Process. Also Brillouin Rayleigh Scatt.* **2006**, *37*, 1381–1392. [[CrossRef](#)]
60. Khan, M.U.; Khalid, M.; Shafiq, I.; Khera, R.A.; Shafiq, Z.; Jawaria, R.; Shafiq, M.; Alam, M.M.; Braga, A.A.C.; Imran, M. Theoretical Investigation of Nonlinear Optical Behavior for Rod and T-Shaped Phenothiazine Based D- $\pi$ -A Organic Compounds and Their Derivatives. *J. Saudi Chem. Soc.* **2021**, *25*, 101339. [[CrossRef](#)]
61. Ali, A.; Kuznetsov, A.; Khan, M.U.; Tahir, M.N.; Ashfaq, M.; Raza, A.R.; Muhammad, S. 2-Amino-6-Methylpyridine Based Co-Crystal Salt Formation Using Succinic Acid: Single-Crystal Analysis and Computational Exploration. *J. Mol. Struct.* **2021**, *1230*, 129893. [[CrossRef](#)]
62. Mahmood, A.; Khan, S.U.-D.; Rana, U.A.; Tahir, M.H. Red Shifting of Absorption Maxima of Phenothiazine Based Dyes by Incorporating Electron-Deficient Thiadiazole Derivatives as  $\pi$ -Spacer. *Arab. J. Chem.* **2019**, *12*, 1447–1453. [[CrossRef](#)]
63. Ali, A.; Khalid, M.; Din, Z.U.; Asif, H.M.; Imran, M.; Tahir, M.N.; Ashfaq, M.; Rodrigues-Filho, E. Exploration of Structural, Electronic and Third Order Nonlinear Optical Properties of Crystalline Chalcone Systems: Monoarylidene and Unsymmetrical Diarylidene Cycloalkanones. *J. Mol. Struct.* **2021**, *1241*, 130685. [[CrossRef](#)]
64. Mahmood, A.; Irfan, A. Effect of Fluorination on Exciton Binding Energy and Electronic Coupling in Small Molecule Acceptors for Organic Solar Cells. *Comput. Theor. Chem.* **2020**, *1179*, 112797. [[CrossRef](#)]
65. Srnec, M.; Solomon, E.I. Frontier Molecular Orbital Contributions to Chlorination versus Hydroxylation Selectivity in the Non-Heme Iron Halogenase SyrB2. *J. Am. Chem. Soc.* **2017**, *139*, 2396–2407. [[CrossRef](#)]
66. Khalid, M.; Shafiq, I.; Zhu, M.; Khan, M.U.; Shafiq, Z.; Iqbal, J.; Alam, M.M.; Braga, A.A.C.; Imran, M. Efficient Tuning of Small Acceptor Chromophores with A1- $\pi$ -A2- $\pi$ -A1 Configuration for High Efficacy of Organic Solar Cells via End Group Manipulation. *J. Saudi Chem. Soc.* **2021**, *25*, 101305. [[CrossRef](#)]
67. Parr, R.G.; Donnelly, R.A.; Levy, M.; Palke, W.E. Electronegativity: The Density Functional Viewpoint. *J. Chem. Phys.* **1978**, *68*, 3801–3807. [[CrossRef](#)]
68. Fukui, K. Role of Frontier Orbitals in Chemical Reactions. *Science* **1982**, *218*, 747–754. [[CrossRef](#)] [[PubMed](#)]
69. Lesar, A.; Milošev, I. Density Functional Study of the Corrosion Inhibition Properties of 1,2,4-Triazole and Its Amino Derivatives. *Chem. Phys. Lett.* **2009**, *483*, 198–203. [[CrossRef](#)]
70. Parthasarathi, R.; Padmanabhan, J.; Elango, M.; Subramanian, V.; Chattaraj, P.K. Intermolecular Reactivity through the Generalized Philicity Concept. *Chem. Phys. Lett.* **2004**, *394*, 225–230. [[CrossRef](#)]
71. Politzer, P.; Truhlar, D.G. Introduction: The Role of the Electrostatic Potential in Chemistry. In *Chemical Applications of Atomic and Molecular Electrostatic Potentials*; Springer: Berlin/Heidelberg, Germany, 1981; pp. 1–6.
72. Parr, R.G.; Pearson, R.G. Absolute Hardness: Companion Parameter to Absolute Electronegativity. *J. Am. Chem. Soc.* **1983**, *105*, 7512–7516. [[CrossRef](#)]
73. Peng, Z.; Yu, L. Second-Order Nonlinear Optical Polyimide with High-Temperature Stability. *Macromolecules* **1994**, *27*, 2638–2640. [[CrossRef](#)]
74. Schmitt, J.; Heitz, V.; Sour, A.; Bolze, F.; Ftouni, H.; Nicoud, J.-F.; Flamigni, L.; Ventura, B. Diketopyrrolopyrrole-Porphyrin Conjugates with High Two-Photon Absorption and Singlet Oxygen Generation for Two-Photon Photodynamic Therapy. *Angew. Chem.* **2015**, *127*, 171–175. [[CrossRef](#)]

75. Khalid, M.; Khan, M.U.; Shafiq, I.; Hussain, R.; Mahmood, K.; Hussain, A.; Jawaria, R.; Hussain, A.; Imran, M.; Assiri, M.A. NLO Potential Exploration for D- $\pi$ -A Heterocyclic Organic Compounds by Incorporation of Various  $\pi$ -Linkers and Acceptor Units. *Arab. J. Chem.* **2021**, *14*, 103295. [CrossRef]
76. Prasad, P.N.; Williams, D.J. *Introduction to Nonlinear Optical Effects in Molecules and Polymers*; Wiley: New York, NY, USA, 1991; Volume 1.
77. Khalid, M.; Arshad, M.N.; Tahir, M.N.; Asiri, A.M.; Naseer, M.M.; Ishaq, M.; Khan, M.U.; Shafiq, Z. An Efficient Synthesis, Structural (SC-XRD) and Spectroscopic (FTIR, <sup>1</sup>HNMR, MS Spectroscopic) Characterization of Novel Benzofuran-Based Hydrazones: An Experimental and Theoretical Studies. *J. Mol. Struct.* **2020**, *1216*, 128318. [CrossRef]
78. Mohandas, T.; Inbaseelan, C.R.D.; Saravanan, S.; Sakthivel, P. Glycine-D-Tartaric Acid (1/1). *Acta Crystallogr. Sect. E Struct. Rep. Online* **2013**, *69*, o236. [CrossRef]
79. Sanz, R.; Martínez, F.; Orcajo, G.; Wojtas, L.; Briones, D. Synthesis of a Honeycomb-like Cu-Based Metal–Organic Framework and Its Carbon Dioxide Adsorption Behaviour. *Dalton Trans.* **2013**, *42*, 2392–2398. [CrossRef] [PubMed]
80. Sheldrick, G.M. A Short History of SHELX. *Acta Crystallogr. A* **2008**, *64*, 112–122. [CrossRef] [PubMed]
81. Kratzert, D.; Holstein, J.J.; Krossing, I. DSR: Enhanced Modelling and Refinement of Disordered Structures with SHELXL. *J. Appl. Crystallogr.* **2015**, *48*, 933–938. [CrossRef]
82. Spek, A.L. Structure Validation in Chemical Crystallography. *Acta Crystallogr. D Biol. Crystallogr.* **2009**, *65*, 148–155. [CrossRef]
83. Macrae, C.F.; Sovago, I.; Cottrell, S.J.; Galek, P.T.; McCabe, P.; Pidcock, E.; Platings, M.; Shields, G.P.; Stevens, J.S.; Towler, M. Mercury 4.0: From Visualization to Analysis, Design and Prediction. *J. Appl. Crystallogr.* **2020**, *53*, 226–235. [CrossRef]
84. Farrugia, L.J. WinGX and ORTEP for Windows: An Update. *J. Appl. Crystallogr.* **2012**, *45*, 849–854. [CrossRef]
85. Frisch, M.; Trucks, G.W.; Schlegel, H.B.; Scuseria, G.E.; Robb, M.A.; Cheeseman, J.R.; Scalmani, G.; Barone, V.; Mennucci, B.; Petersson, G.A. *Gaussian 09, Revision D. 01 2009*; Gaussian: Wallingford, CT, USA, 2009.
86. Zhao, Y.; Truhlar, D.G. The M06 Suite of Density Functionals for Main Group Thermochemistry, Thermochemical Kinetics, Noncovalent Interactions, Excited States, and Transition Elements: Two New Functionals and Systematic Testing of Four M06-Class Functionals and 12 Other Functionals. *Theor. Chem. Acc.* **2008**, *120*, 215–241. [CrossRef]
87. Khalid, M.; Ali, A.; Rehman, M.F.U.; Mustaqem, M.; Ali, S.; Khan, M.U.; Asim, S.; Ahmad, N.; Saleem, M. Exploration of Noncovalent Interactions, Chemical Reactivity, and Nonlinear Optical Properties of Piperidone Derivatives: A Concise Theoretical Approach. *ACS Omega* **2020**, *5*, 13236–13249. [CrossRef] [PubMed]
88. Glendenning, E.D.; Reed, A.E.; Carpenter, J.E.; Weinhold, F. *Nbo Version 3.1, Tci*; University of Wisconsin–Madison: Madison, WI, USA, 1998; Volume 65.
89. Dennington, R.; Keith, T.; Millam, J. *GaussView, Version 5*; Semichem Inc.: Shawnee, KS, USA, 2009.
90. O'boyle, N.M.; Tenderholt, A.L.; Langner, K.M. Cclib: A Library for Package-Independent Computational Chemistry Algorithms. *J. Comput. Chem.* **2008**, *29*, 839–845. [CrossRef] [PubMed]
91. Zhurko, G.A. Chemcraft. *Receiv. Oct.* **2014**, *22*. Available online: <http://www.chemcraftprog.com> (accessed on 19 March 2023).
92. Hanwell, M.D.; Curtis, D.E.; Lonie, D.C.; Vandermeersch, T.; Zurek, E.; Hutchison, G.R. Avogadro: An Advanced Semantic Chemical Editor, Visualization, and Analysis Platform. *J. Cheminform.* **2012**, *4*, 17. [CrossRef]

**Disclaimer/Publisher's Note:** The statements, opinions and data contained in all publications are solely those of the individual author(s) and contributor(s) and not of MDPI and/or the editor(s). MDPI and/or the editor(s) disclaim responsibility for any injury to people or property resulting from any ideas, methods, instructions or products referred to in the content.